International Applied Mechanics, Vol. 45, No. 1, 2009

ACTIVE DAMPING OF THE FORCED VIBRATION OF A HINGED BEAM WITH PIEZOELECTRIC LAYERS, GEOMETRICAL AND PHYSICAL NONLINEARITIES TAKEN INTO ACCOUNT

Ya. A. Zhuk[1] and I. A. Guz[2]

The problem of forced vibration of a hinged beam with piezoelectric layers is solved. Issues of mechanical and electric excitation of vibration and the possibility of damping mechanically induced vibration by applying a voltage to the electrodes of the piezolayers are studied. The effect of the physically nonlinear behavior of the passive layers on the response of the sensor layer and entire structure and the effect of geometric nonlinearity on the behavior of the structure and sensor layer are analyzed. The interaction of physical and geometrical nonlinearities for transient and stationary processes is studied

Keywords: piezoelectric materials, physical nonlinearity, geometrical nonlinearity, forced vibration, layered beam, damping of vibration

Introduction. The stringent requirements to modern complex devices have recently compelled many researchers to pay attention to the modeling and control of the vibration of flexible structures [2–4, 12–17]. The rapid development of the modern technology necessitates changing over from the traditional methods of vibration control to new ones that allow implementing more complex and highly effective operating modes and observing numerous life and reliability criteria. As a result, the modeling of the vibration of flexible structures and their elements and study of the possibilities for controlling them have gained a new impetus and are aimed at the development of systems with improved or qualitatively new characteristics. The ultimate goal of such studies is to create a new generation of active adaptive materials capable of responding to an external load according to predefined criteria or a program and having the functions of self-checking, self-diagnostics, and self-restoration [19].

Currently, structronics is the most intensively developing division of mechanics. It is concerned with electroelastic systems, active materials, and control of the vibration of structures made of various materials [22]. For example, there is a variety of materials having specific properties (piezoelectric materials, materials with shape memory, materials with electrostrictive, electromagnetoelastic, and other electrorheological properties) that are widely used for the active control of vibration [19]. Of them, the most popular are piezoelectric materials used as sensors or actuators due to the direct and inverse piezoelectric effects [5, 6, 17].

Piezoelectric elements are most often used as distributed sensors or actuators (or their combinations) [1–4, 13–16, 21]. Modeling the vibration and control of elements with such distributed sensors and actuators is, as a rule, reduced to problems for layered beams, plates, or shells containing or partially or completely covered with piezoactive layers [1–4, 13–16, 21–23]. A piezoelectric layer can be used as a distributed sensor due to the direct piezoelectric effect, and by applying a high external voltage to this layer, we can excite or control (what an actuator does) vibration due to the inverse piezoelectric effect. These vibrations may be shifted in phase with respect to the external, say, mechanical load to compensate for undesirable displacements.

[1]S. P. Timoshenko Institute of Mechanics, National Academy of Sciences of Ukraine, 3 Nesterov St., Kyiv, Ukraine 03057, e-mail: term@inmech.kiev.ua. [2]Center for Micro- and Nanomechanics, University of Aberdeen, AB24 3UE Aberdeen, Scotland, e-mail: i.guz@abdn.ac.uk. Translated from Prikladnaya Mekhanika, Vol. 45, No. 1, pp. 118–136, January 2009. Original article submitted April 21, 2008.

 1063-7095/09/4501-0094

In studying the control of the vibration of such systems, one has to consider a wide variety of issues: modeling of the mechanical response and analysis of the strength of electrically passive layered elements and composite materials [11] and description of the coupled electromechanical behavior of piezomaterials [5, 6, 10, 12]; development of theories of multilayer beams, plates, and shells with piezoelectric layers, taking anisotropy into account [1, 21–24]; development of theories of sensors and actuators [3, 4]; problems of sensitivity of sensors [19, 21]; problems of modal control and optimal arrangement of sensors (actuators) [21, 22, 24]; development and optimization of feedback systems [23]; development of nonlinear theories and study of the interaction of various nonlinear factors [25]; allowance for thermal effects [1, 2, 21, 22]. Some of the issues are well understood, while others (for example, nonlinear effects and temperature) require additional study. Quite extensive reviews of the current state of the art in the active control of vibration of mechanical systems can be found in [17, 19, 21].

Publications on active control are restricted to elastic models of electrically active and passive materials. To describe dissipation, the equation of motion, as a rule, includes additional terms proportional to the velocity and responsible for viscous friction. Such an approach appears justified to apply to systems with combined (active and passive) control of vibration [17, 19]. To describe the real behavior of piezoelectric, and, especially, electrically passive materials, it is necessary to use more complex models of materials exhibiting physically nonlinear reaction to an external load. Indeed, elastoplastic and (if velocity is high) viscoelastic dampers are used to suppress vibration with high amplitudes, including intensive shock or other impulsive loads.

Intensive loading may also cause large deflections. The membrane force may appear large because of the boundary conditions (hinging, clamping). In such cases, it is important to describe the interaction between and the effect of geometrical and physical nonlinearities on the behavior of a layered structure with piezoelectric components, to analyze changes in the sensor readings, and to study the steady-state residual vibrations after applying a voltage to balance the external mechanical load.

For these purposes, the present paper models the forced vibration of a hinged sandwich beam with the core layer made of aluminum alloy and the face layers of piezoceramics. The behavior of the electrically passive (no piezoelectric effect) aluminum alloy is characterized by the Bodner–Partom model [8, 9], which describes the physically nonlinear response of a material based on the concept of internal variables. To this end, use is made of a set of internal variables that describe all inelastic effects: isotropic and kinematic hardening, stress relaxation, Bauschinger effect, etc. The piezoceramic layers are elastic and transversely isotropic. We will address the issues of mechanical and electric excitation, the possibility of damping mechanically excited vibrations by applying the appropriate potential difference to the electrodes of the piezolayers, the influence of the physically nonlinear behavior of the passive layers on the response of the piezoelectric layer and the entire structure, the influence of geometrical nonlinearity on the behavior of the structure and piezoelectric layer, and the interaction of the physical and geometrical nonlinearities during both transient and steady-state vibrations.

1. General Equations of Electroelasticity for Thin-Walled Elements with Physically Nonlinear Piezoactive Layers. The theory of piezoelectric effect has long been developed and is well understood now. In the isothermal case, the constitutive equations for linear piezoelectric materials can be written in the following form [5, 6, 22]:

$$\sigma_{ij} = c^{\mathrm{D}}_{ijkl}\varepsilon_{kl} - h_{mij}D_m, \quad E_n = \beta^{\mathrm{S}}_{nm}D_m - h_{nkl}\varepsilon_{kl} \quad (i, j, k, l, m, n = 1, 2, 3), \tag{1.1}$$

where σ_{ij} and ε_{ij} are the stress and strain tensors; E_i and D_i are the electric-field intensity and electric-flux density (charge per unit area), respectively; c^{D}_{ijkl} are the elastic moduli at constant electric-flux density; h_{ijk} are the piezoelectric constants; and β^{S}_{ij} is the permittivity matrix at constant strain. These equations have been derived in quasistatic approximation, i.e., the equations of electrostatics [5, 6] are considered to hold.

Equations (1.1) are much simpler for thin-walled structures [1, 2]. We will use the equations of electroelasticity derived in [1, 2] for layered shells made of piezoelectric materials that are transversely isotropic in the polarization direction (thickness coordinate) and physically nonlinear. Similar equations for layered shells made of orthotropic piezoelectric viscoelastic materials were derived in [3, 4].

Let us consider multilayer shells with layers of constant thickness. The layers are in perfect contact with each other. The piezoelectric layers are covered with infinitely thin electrodes to which an electric potential difference can be applied. The shell is described in an orthogonal coordinate system (α, β, γ). The surface equidistant to the surfaces of the layers is chosen to be the reference one. The γ-axis is normal to the reference surface. The position of a point on this surface is defined by orthogonal coordinates α and β measured along the lines of principal curvature. The layers are numbered in the γ-direction. The coordinate of the upper surface of the sth layer is denoted by γ_s.

Assume that the total strain can be represented by the sums of elastic ($\varepsilon_{\alpha\beta}^{el}$) and inelastic ($\varepsilon_{\alpha\beta}^{pl}$) components: $\varepsilon_{\alpha\beta} = \varepsilon_{\alpha\beta}^{el} + \varepsilon_{\alpha\beta}^{pl}$.

The general equations of state (1.1) for a transversely isotropic body prepolarized in the γ-direction can be written in the following form [1, 2]:

$$\sigma_{\alpha\alpha} = c_{11}^{D}(\varepsilon_{\alpha\alpha} - \varepsilon_{\alpha\alpha}^{pl}) + c_{12}^{D}(\varepsilon_{\beta\beta} - \varepsilon_{\beta\beta}^{pl}) + c_{13}^{D}(\varepsilon_{\gamma\gamma} - \varepsilon_{\gamma\gamma}^{pl}) - h_{31}D_{\gamma},$$

$$\sigma_{\alpha\beta} = 1/2(c_{11}^{D} - c_{12}^{D})(\varepsilon_{\alpha\beta} - \varepsilon_{\alpha\beta}^{pl}),$$

$$\sigma_{\beta\beta} = c_{12}^{D}(\varepsilon_{\alpha\alpha} - \varepsilon_{\alpha\alpha}^{pl}) + c_{11}^{D}(\varepsilon_{\beta\beta} - \varepsilon_{\beta\beta}^{pl}) + c_{13}^{D}(\varepsilon_{\gamma\gamma} - \varepsilon_{\gamma\gamma}^{pl}) - h_{31}D_{\gamma},$$

$$\sigma_{\alpha\gamma} = c_{44}^{D}(\varepsilon_{\alpha\gamma} - \varepsilon_{\alpha\gamma}^{pl}) - h_{15}D_{\beta},$$

$$\sigma_{\gamma\gamma} = c_{13}^{D}(\varepsilon_{\alpha\alpha} - \varepsilon_{\alpha\alpha}^{pl}) + c_{13}^{D}(\varepsilon_{\beta\beta} - \varepsilon_{\beta\beta}^{pl}) + c_{33}^{D}(\varepsilon_{\gamma\gamma} - \varepsilon_{\gamma\gamma}^{pl}) - h_{33}D_{\gamma},$$

$$\sigma_{\beta\gamma} = c_{44}^{D}(\varepsilon_{\beta\gamma} - \varepsilon_{\beta\gamma}^{pl}) - h_{15}D_{\alpha},$$

$$E_{\alpha} = -h_{51}(\varepsilon_{\alpha\gamma} - \varepsilon_{\alpha\gamma}^{pl}) + \beta_{11}^{S}D_{\alpha}, \quad E_{\beta} = -h_{51}(\varepsilon_{\beta\gamma} - \varepsilon_{\beta\gamma}^{pl}) + \beta_{11}^{S}D_{\beta},$$

$$E_{\gamma} = -h_{31}(\varepsilon_{\alpha\alpha} - \varepsilon_{\alpha\alpha}^{pl} + \varepsilon_{\beta\beta} - \varepsilon_{\beta\beta}^{pl}) + \beta_{33}^{S}D_{\gamma}. \tag{1.2}$$

Let us use the standard Kirchhoff–Love hypotheses generalized to the case of electroelasticity and plane stress state [1–4, 20]:

$$\sigma_{\alpha\gamma} = \sigma_{\beta\gamma} = \sigma_{\alpha\beta} = 0, \quad \sigma_{\gamma\gamma} = 0, \quad D_{\alpha} = D_{\beta} = 0, \quad D_{\gamma} = D_{\gamma}(\alpha, \beta). \tag{1.3}$$

The hypothesis $\sigma_{\gamma\gamma} = 0$ and the plastic incompressibility condition $\varepsilon_{kk}^{pl} = 0$ $(k = \alpha, \beta, \gamma)$ yield an expression for $\varepsilon_{\gamma\gamma}$:

$$\varepsilon_{\gamma\gamma} = \left(-c_{13}^{D}(\varepsilon_{\alpha\alpha} + \varepsilon_{\beta\beta}) + (c_{13} - c_{33})(\varepsilon_{\alpha\alpha}^{pl} + \varepsilon_{\beta\beta}^{pl}) + h_{33}D_{\gamma}\right)(c_{33}^{D})^{-1}. \tag{1.4}$$

Substituting (1.4) into Eqs. (1.2) and taking (1.3) into account, we obtain

$$\sigma_{\alpha\alpha} = \bar{c}_{11}(\varepsilon_{\alpha\alpha} - \varepsilon_{\alpha\alpha}^{pl}) + \bar{c}_{12}(\varepsilon_{\beta\beta} - \varepsilon_{\beta\beta}^{pl}) - \bar{h}_{31}D_{\gamma},$$

$$\sigma_{\beta\beta} = \bar{c}_{12}(\varepsilon_{\alpha\alpha} - \varepsilon_{\alpha\alpha}^{pl}) + \bar{c}_{11}(\varepsilon_{\beta\beta} - \varepsilon_{\beta\beta}^{pl}) - \bar{h}_{31}D_{\gamma},$$

$$\sigma_{\alpha\beta} = \bar{c}_{66}\varepsilon_{\alpha\beta} - \bar{c}_{66}\varepsilon_{\alpha\beta}^{pl}, \tag{1.5}$$

$$E_{\gamma} = -\bar{h}_{31}(\varepsilon_{\alpha\alpha} + \varepsilon_{\beta\beta}) + \bar{h}_{31}(\varepsilon_{\alpha\alpha}^{pl} + \varepsilon_{\beta\beta}^{pl}) + \bar{\beta}_{33}^{S}D_{\gamma}, \tag{1.6}$$

where

$$\bar{c}_{11} = c_{11}^{D} - (c_{13}^{D})^2 / c_{33}^{D}, \quad \bar{c}_{12} = c_{12}^{D} - (c_{13}^{D})^2 / c_{33}^{D}, \quad \bar{c}_{66} = 1/2(c_{11}^{D} - c_{12}^{D}),$$

$$\bar{h}_{31} = p(h_{31} - h_{33}c_{13}^{D}) / c_{33}^{D}, \quad \bar{\beta}_{33}^{S} = \beta_{33}^{S} - h_{33}^{2} / c_{33}^{D} \tag{1.7}$$

in the plane case.

The coefficient p is equal to 1 if the prepolarization vector coincides with the positive direction of the γ-axis and is equal to –1 otherwise.

Using the Kirchhoff–Love hypothesis, we can express the displacement components $\{u^\gamma, v^\gamma, w^\gamma\}$ of an arbitrary point of the shell in terms of the displacement components $\{u, v, w\}$ of the reference surface as follows [1, 2]: $u^\gamma = u + \gamma\vartheta_1$, $v^\gamma = v + \gamma\vartheta_2$, $w^\gamma = w - \gamma(\vartheta_1^2 + \vartheta_2^2)/2$, where u, v, w, ϑ_1, and ϑ_2 are functions of α and β, and $\vartheta_1 = -1/A\partial w/\partial\alpha + u/R_1$, $\vartheta_2 = -1/B\partial w/\partial\beta + v/R_2$, $R_{1,2}$ are the principal radii of curvature; and A and B are the Lamé constants.

The strain components are expressed as

$$\varepsilon_{\alpha\alpha} = \varepsilon_1 + \gamma\kappa_1, \quad \varepsilon_{\beta\beta} = \varepsilon_2 + \gamma\kappa_2, \quad \varepsilon_{\alpha\beta} = \varepsilon_{12} + 2\gamma\kappa_{12}, \tag{1.8}$$

where

$$\varepsilon_1 = \varepsilon_{1L} + \varepsilon_{1N}, \quad \varepsilon_2 = \varepsilon_{2L} + \varepsilon_{2N}, \quad \varepsilon_{12} = \varepsilon_{12L} + \varepsilon_{12N},$$

$$\kappa_1 = \kappa_{1L} + \kappa_{1N}, \quad \kappa_2 = \kappa_{2L} + \kappa_{2N}, \quad \kappa_{12} = 2\kappa_{12L} + 2\kappa_{12N},$$

$$\varepsilon_{1L} = \frac{1}{A}\frac{\partial u}{\partial\alpha} + \frac{v}{AB}\frac{\partial A}{\partial\beta} + \frac{w}{R_1}, \quad \varepsilon_{2L} = \frac{1}{B}\frac{\partial v}{\partial\beta} + \frac{u}{AB}\frac{\partial B}{\partial\alpha} + \frac{w}{R_2}, \quad \varepsilon_{12L} = \frac{A}{B}\frac{\partial}{\partial\beta}\left(\frac{u}{A}\right) + \frac{B}{A}\frac{\partial}{\partial\alpha}\left(\frac{v}{B}\right),$$

$$\varepsilon_{1N} = \frac{1}{2}\vartheta_1^2, \quad \varepsilon_{2N} = \frac{1}{2}\vartheta_2^2, \quad \varepsilon_{12N} = \vartheta_1\vartheta_2,$$

$$\kappa_{1L} = \frac{1}{A}\frac{\partial\vartheta_1}{\partial\alpha} + \frac{\vartheta_2}{AB}\frac{\partial A}{\partial\beta}, \quad \kappa_{2L} = \frac{1}{B}\frac{\partial\vartheta_2}{\partial\beta} + \frac{\vartheta_1}{AB}\frac{\partial B}{\partial\alpha}, \quad 2\kappa_{12L} = \tau_1 + \tau_2,$$

$$\tau_1 = \frac{1}{A}\frac{\partial\vartheta_2}{\partial\alpha} - \frac{\vartheta_1}{AB}\frac{\partial A}{\partial\beta} - \frac{\omega_1}{R_1}, \quad \tau_2 = \frac{1}{B}\frac{\partial\vartheta_1}{\partial\beta} - \frac{\vartheta_2}{AB}\frac{\partial B}{\partial\alpha} - \frac{\omega_2}{R_2},$$

$$\omega_1 = \frac{1}{A}\frac{\partial v}{\partial\alpha} - \frac{u}{AB}\frac{\partial A}{\partial\beta}, \quad \omega_2 = \frac{1}{B}\frac{\partial u}{\partial\beta} - \frac{v}{AB}\frac{\partial B}{\partial\alpha},$$

$$\kappa_{1N} = -\frac{\vartheta_2^2}{2R_1}, \quad \kappa_{2N} = -\frac{\vartheta_1^2}{2R_2}, \quad 2\kappa_{12N} = 0.$$

In what follows, we will neglect the curvatures and twists in the first approximation: $\kappa_{1N} = \kappa_{2N} = 0$.

Statically equivalent forces and moments per unit arc lengths of the coordinate lines of the original surface are defined in an ordinary manner [1–4].

Integrating expressions (1.5) over the thickness of the shell and taking (1.8) into account, we obtain constitutive equations [1, 2]:

$$N_1 = C_{11}\varepsilon_{1L} + C_{12}\varepsilon_{2L} + K_{11}\kappa_1 + K_{12}\kappa_2 + N_{pl1} + N_E + N_{G1},$$

$$N_2 = C_{12}\varepsilon_{1L} + C_{11}\varepsilon_{2L} + K_{12}\kappa_1 + K_{11}\kappa_2 + N_{pl2} + N_E + N_{G2},$$

$$M_1 = K_{11}\varepsilon_{1L} + K_{12}\varepsilon_{2L} + D_{11}\kappa_1 + D_{12}\kappa_2 + M_{pl1} + M_E + M_{G1},$$

$$M_2 = K_{12}\varepsilon_{1L} + K_{11}\varepsilon_{2L} + D_{12}\kappa_1 + D_{11}\kappa_2 + M_{pl2} + M_E + M_{G1},$$

$$S = N_{12} - M_{21}/R_2 = N_{21} - M_{12}/R_1 = C_{66}\varepsilon_{12L} + 2K_{66}\kappa_{12} - N_{pl12} + N_{G12},$$

$$H = (M_{12} - M_{21})/2 = K_{66}\varepsilon_{12L} + 2D_{66}\kappa_{12} - M_{pl12} + M_{G12}, \tag{1.9}$$

where

$$C_{11} = \sum_s (C_{11}^{(s)} - l_{33}^{(s)-1} n^{(s)} n^{(s)}), \quad C_{12} = \sum_s (C_{12}^{(s)} - l_{33}^{(s)-1} n^{(s)} n^{(s)}),$$

$$K_{11} = \sum_s (K_{11}^{(s)} - l_{33}^{(s)-1} n^{(s)} m^{(s)}), \quad K_{12} = \sum_s (K_{12}^{(s)} - l_{33}^{(s)-1} n^{(s)} m^{(s)}),$$

$$D_{11} = \sum_s (D_{11}^{(s)} - l_{33}^{(s)-1} m^{(s)} m^{(s)}), \quad D_{12} = \sum_s (D_{12}^{(s)} - l_{33}^{(s)-1} m^{(s)} m^{(s)}),$$

$$C_{66} = \sum_s C_{66}^{(s)}, \quad K_{66} = \sum_s K_{66}^{(s)}, \quad D_{66} = \sum_s D_{66}^{(s)},$$

$$N_{\text{pl}1} = \sum_s \left(\int_{\gamma_{s-1}}^{\gamma_s} (-\bar{c}_{11} \varepsilon_{11}^{\text{pl}} - \bar{c}_{12} \varepsilon_{22}^{\text{pl}}) d\gamma - \frac{n^{(s)} N_{\text{pl}}^{(s)}}{l_{33}^{(s)}} \right), \quad N_{\text{pl}2} = \sum_s \left(\int_{\gamma_{s-1}}^{\gamma_s} (-\bar{c}_{12} \varepsilon_{11}^{\text{pl}} - \bar{c}_{11} \varepsilon_{22}^{\text{pl}}) d\gamma - \frac{n^{(s)} N_{\text{pl}}^{(s)}}{l_{33}^{(s)}} \right),$$

$$M_{\text{pl}1} = \sum_s \left(\int_{\gamma_{s-1}}^{\gamma_s} (-\bar{c}_{11} \varepsilon_{11}^{\text{pl}} - \bar{c}_{12} \varepsilon_{22}^{\text{pl}}) \gamma d\gamma - \frac{m^{(s)} N_{\text{pl}}^{(s)}}{l_{33}^{(s)}} \right), \quad M_{\text{pl}2} = \sum_s \left(\int_{\gamma_{s-1}}^{\gamma_s} (-\bar{c}_{12} \varepsilon_{11}^{\text{pl}} - \bar{c}_{11} \varepsilon_{22}^{\text{pl}}) \gamma d\gamma - \frac{m^{(s)} N_{\text{pl}}^{(s)}}{l_{33}^{(s)}} \right),$$

$$N_{\text{pl}12} = \sum_s \int_{\gamma_{s-1}}^{\gamma_s} \bar{c}_{66} \varepsilon_{12}^{\text{pl}} d\gamma, \quad M_{\text{pl}12} = \sum_s \int_{\gamma_{s-1}}^{\gamma_s} \bar{c}_{66} \varepsilon_{12}^{\text{pl}} \gamma d\gamma,$$

$$N_{G1} = \sum_s \left(\int_{\gamma_{s-1}}^{\gamma_s} (\bar{c}_{11} \varepsilon_{1N} + \bar{c}_{12} \varepsilon_{2N}) d\gamma + \frac{n^{(s)} N_G^{(s)}}{l_{33}^{(s)}} \right), \quad N_{G2} = \sum_s \left(\int_{\gamma_{s-1}}^{\gamma_s} (\bar{c}_{12} \varepsilon_{1N} + \bar{c}_{22} \varepsilon_{2N}) d\gamma + \frac{n^{(s)} N_G^{(s)}}{l_{33}^{(s)}} \right),$$

$$M_{G1} = \sum_s \left(\int_{\gamma_{s-1}}^{\gamma_s} (\bar{c}_{11} \varepsilon_{1N} + \bar{c}_{12} \varepsilon_{2N}) \gamma d\gamma + \frac{m^{(s)} N_G^{(s)}}{l_{33}^{(s)}} \right), \quad M_{G2} = \sum_s \left(\int_{\gamma_{s-1}}^{\gamma_s} (\bar{c}_{12} \varepsilon_{1N} + \bar{c}_{22} \varepsilon_{2N}) \gamma d\gamma + \frac{m^{(s)} N_G^{(s)}}{l_{33}^{(s)}} \right),$$

$$N_{G12} = \sum_s \int_{\gamma_{s-1}}^{\gamma_s} \bar{c}_{66} \varepsilon_{12N} d, \quad M_{G12} = \sum_s \int_{\gamma_{s-1}}^{\gamma_s} \bar{c}_{66} \varepsilon_{12N} \gamma d\gamma,$$

$$N_E = \sum_s \left(\frac{n^{(s)} U^{(s)}}{l_{33}^{(s)}} \right), \quad M_E = \sum_s \left(\frac{m^{(s)} U^{(s)}}{l_{33}^{(s)}} \right). \tag{1.10}$$

$$C_{1i}^{(s)} = \int_{\gamma_{s-1}}^{\gamma_s} \bar{c}_{1i} d\gamma, \quad K_{1i}^{(s)} = \int_{\gamma_{s-1}}^{\gamma_s} \bar{c}_{1i} \gamma d\gamma, \quad D_{1i}^{(s)} = \int_{\gamma_{s-1}}^{\gamma_s} \bar{c}_{1i} \gamma^2 d\gamma, \quad C_{66}^{(s)} = \int_{\gamma_{s-1}}^{\gamma_s} \bar{c}_{66} d\gamma,$$

$$K_{66}^{(s)} = \int_{\gamma_{s-1}}^{\gamma_s} \bar{c}_{66} \gamma d\gamma, \quad D_{66}^{(s)} = \int_{\gamma_{s-1}}^{\gamma_s} \bar{c}_{66} \gamma^2 d\gamma, \quad n^{(s)} = \int_{\gamma_{s-1}}^{\gamma_s} \bar{h}_{31} d\gamma, \quad m^{(s)} = \int_{\gamma_{s-1}}^{\gamma_s} \bar{h}_{31} \gamma d\gamma,$$

$$N_{\text{pl}}^{(s)} = \int_{\gamma_{s-1}}^{\gamma_s} \bar{h}_{31} (\varepsilon_{11}^{\text{pl}} + \varepsilon_{22}^{\text{pl}}) d\gamma, \quad N_G^{(s)} = \int_{\gamma_{s-1}}^{\gamma_s} \bar{h}_{31} (\varepsilon_{1N} + \varepsilon_{2N}) d\gamma \quad (i = 1, 2). \tag{1.11}$$

In deriving formulas (1.9)–(1.11), the electric-flux density $D_\gamma^{(s)}$ is expressed in terms of the potential difference $U^{(s)}$ across the surface electrodes of the piezoelectric layers. For example, integrating Eq. (1.6) over the layer thickness, we obtain

$$D_\gamma^{(s)} = l_{33}^{(s)-1}\left[-V^{(s)} + n^{(s)}(\varepsilon_{1L} + \varepsilon_{2L}) + m^{(s)}(\kappa_1 + \kappa_2) - N_{\text{pl}}^{(s)} + N_G^{(s)}\right] / l_{33}^{(s)}, \tag{1.12}$$

where

$$l_{33}^{(s)} = \int_{\gamma_{s-1}}^{\gamma_s} \bar{\beta}_{33}^s \, d\gamma, \quad V^{(s)} = -\int_{\gamma_{s-1}}^{\gamma_s} E_\gamma \, d\gamma. \tag{1.13}$$

Note that Eqs. (1.9) have the most general form. For the passive layers, which can undergo plastic deformation, it is necessary to equate all electric terms to zero: $\bar{h}_{31} = 0$.

For the piezoelectric layers, which deform elastically, Eqs. (1.9) are used with the conditions

$$N_{\text{pl}1} = N_{\text{pl}2} = N_{\text{pl}12} = M_{\text{pl}1} = M_{\text{pl}2} = M_{\text{pl}12} = 0.$$

To analyze the behavior of the sth piezolayer as a sensor and to assess the electric current in its electrodes, it is necessary to use formula (1.12) and the following relation [5, 6]:

$$\frac{d}{dt}\iint_{S_1^+} (\vec{n}\cdot\vec{D})\, dS = -I(t), \tag{1.14}$$

which follows from the fact that the total charge Q on the electrode is expressed in terms of the normal component of the electric-flux density $\vec{D}$ as

$$Q = -\iint_{S_1^+} (\vec{n}\cdot\vec{D})\, dS,$$

where $I(t)$ is the electric current; S_1^+ is the area of one of the layer surfaces; and $\vec{n}$ is the outward normal vector to this surface.

The equations of motion of thin-walled shells are presented in [1–4]. Together with appropriate boundary and initial conditions, they constitute the statement of the nonstationary problem of electroelasticity for layered shells with piezoelectric layers.

2. Model of Physically Nonlinear Material. The piezoactive and passive layers are selected so that their elastic moduli are in a definite ratio. The moduli may be chosen approximately equal for an actuator to maintain a reliable effect on the passive element. For a sensor, more important is the received signal and the minimum effect on the stiffness characteristics of the structure or desirable increase in stiffness. The passive layers may deform inelastically under a load of certain levels. To model both elastic and physically nonlinear behavior of the material, use is made of the Bodner–Partom model [8, 9] based on the concept of internal state variables. Let us briefly present the formulas of the model.

The total strain can be represented as the sum of elastic and inelastic terms:

$$\varepsilon_{ij} = \varepsilon_{ij}^{\text{el}} + \varepsilon_{ij}^{\text{pl}}. \tag{2.1}$$

The model also includes the following equations:

Hooke's law

$$s_{ij} = 2G(e_{ij} - \varepsilon_{ij}^{\text{pl}}), \quad \sigma_{kk} = 3K_V(\varepsilon_{kk} - \varepsilon_{kk}^{\theta}), \tag{2.2}$$

where s_{ij} and e_{ij} are the stress and strain deviators, respectively; K_V and G are the bulk and shear moduli, respectively; summation is assumed over repeated indices;

the flow rule with the plastic incompressibility condition

$$\dot{\varepsilon}_{ij}^{\text{pl}} = \lambda s_{ij}, \quad \dot{\varepsilon}_{kk}^{\text{pl}} = 0, \tag{2.3}$$

the kinetic equation

$$D_2^{\mathrm{pl}} = D_0^2 \exp\left[-\left(\frac{Z^2}{3J_2}\right)^n\right], \tag{2.4}$$

where $Z = K + D$, $D_2^{\mathrm{pl}} = \frac{1}{2}\dot{\varepsilon}_{ij}^{\mathrm{pl}}\dot{\varepsilon}_{ij}^{\mathrm{pl}}$, $D_2^{\mathrm{pl}} = \frac{1}{2}\dot{\varepsilon}_{ij}^{\mathrm{pl}}\dot{\varepsilon}_{ij}^{\mathrm{pl}}$, $\lambda^2 = D_2^{\mathrm{pl}} / J_2$; the evolutionary equations for the internal variables responsible for isotropic (K) and kinematic (β_{ij}) hardening:

$$\dot{K} = m_1(K_1 - K)\dot{W}_{\mathrm{pl}}, \quad K(0) = K_0, \quad \dot{\beta}_{ij} = m_2(D_1 u_{ij} - \beta_{ij})\dot{W}_{\mathrm{pl}}, \quad \beta_{ij}(0) = 0, \tag{2.5}$$

where $D = \beta_{ij} u_{ij}$, $u_{ij} = \sigma_{ij} / (\sigma_{ij}\sigma_{ij})^{1/2}$, $\dot{W}_{\mathrm{pl}} = \sigma_{ij}\dot{\varepsilon}_{ij}^{\mathrm{pl}}$; and D_0, D_1, K_0, K_1, m_1, m_2, and n are the model parameters [8, 9].

3. Equations of Electroelasticity for a Beam with Piezoelectric Physically Nonlinear Layers. Consider a layered beam with piezoelectric layers. For the issues being examined, a beam is the simplest object that allows us to analyze the behavior of layered thin-walled structures, the interaction of physical and geometrical nonlinearities, and the capabilities for active damping of forced vibrations [17].

Let us introduce a Cartesian coordinate system ($Oxyz$) so that the beam axis is aligned with the abscissa axis, the thickness coordinate is measured along the z-axis, and the width coordinate along the ordinate axis. Beam geometry: length L (end coordinates: $x = 0$, $x = L$), thickness h (the upper and lower edges: $z = h/2$, $z = -h/2$), width b_y.

The constitutive equations (1.5), (1.6) for the sth layer made of a physically nonlinear piezoelectric material are written in the form

$$\sigma_{xx}^{(s)} = C_{11}^{(s)}\varepsilon_{xx} - C_{11}^{(s)}\varepsilon_{xx}^{\mathrm{pl}} + pH_{31}^{(s)}D_z, \quad E_z^{(s)} = pH_{31}^{(s)}\varepsilon_{xx} - pH_{31}^{(s)}\varepsilon_{xx}^{\mathrm{pl}} + B_{33}^{(s)}D_z, \tag{3.1}$$

where

$$C_{11}^{(s)} = \frac{(c_{11}^{\mathrm{D}} - c_{12}^{\mathrm{D}})[c_{33}^{\mathrm{D}}(c_{11}^{\mathrm{D}} + c_{12}^{\mathrm{D}}) - 2(c_{13}^{\mathrm{D}})^2]}{c_{11}^{\mathrm{D}}c_{33}^{\mathrm{D}} - (c_{13}^{\mathrm{D}})^2}, \quad H_{31}^{(s)} = \frac{(c_{11}^{\mathrm{D}} - c_{12}^{\mathrm{D}})(h_{31}c_{33}^{\mathrm{D}} - h_{33}c_{13}^{\mathrm{D}})}{c_{11}^{\mathrm{D}}c_{33}^{\mathrm{D}} - (c_{13}^{\mathrm{D}})^2},$$

$$B_{33}^{(s)} = \frac{2h_{33}h_{31}c_{13}^{\mathrm{D}} - h_{33}^2 c_{11}^{\mathrm{D}} - h_{31}^2 c_{33}^{\mathrm{D}} + \beta_{33}^{\mathrm{S}}(c_{11}^{\mathrm{D}}c_{33}^{\mathrm{D}} - (c_{13}^{\mathrm{D}})^2)}{c_{11}^{\mathrm{D}}c_{33}^{\mathrm{D}} - (c_{13}^{\mathrm{D}})^2}, \tag{3.2}$$

and the elastic moduli, piezoelectric constants, and permittivity coefficients correspond to the material of this layer.

Following formulas (1.8), we assume that the strains at an arbitrary point of the beam can be defined by the formula below [1, 2]:

$$\varepsilon_{xx} = \varepsilon + z\kappa + \vartheta^2 / 2, \tag{3.3}$$

where ε, κ, and ϑ are the strain of the beam axis, curvature, and angle of rotation of the cross-section, respectively.

Note that formula (3.3) includes geometrical nonlinearity (squared angles of rotation).

The second formula in (1.13) with (3.3) allows us to express the potential difference across the electrodes of a layer as follows:

$$V^{(s)} = n^{(s)}\varepsilon + m^{(s)}\kappa + n^{(s)}\vartheta^2 / 2 + l^{(s)}D_z + R_{\mathrm{pl}}^{(s)}, \tag{3.4}$$

where $n^{(s)} = \int_{z_{s-1}}^{z_s}(-p)H_{31}^{(s)}dz$, $m^{(s)} = \int_{z_{s-1}}^{z_s}(-p)H_{31}^{(s)}zdz$, $l^{(s)} = \int_{z_{s-1}}^{z_s}(-B_{33}^{(s)})dz$, $R_{\mathrm{pl}}^{(s)} = \int_{z_{s-1}}^{z_s}pH_{31}^{(s)}\varepsilon_{xx}^{\mathrm{pl}}dz$.

The first equation in (3.1) and Eq. (3.4) yield expressions for the axial force $N^{(s)}$ and moment $M^{(s)}$ in a layer:

$$N^{(s)} = C_1^{(s)}\varepsilon + K_1^{(s)}\kappa + C_1^{(s)}\vartheta^2 / 2 - n^{(s)}D_z - N_{\mathrm{pl}}^{(s)},$$

$$M^{(s)} = K_1^{(s)}\varepsilon + D_1^{(s)}\kappa + K_1^{(s)}\vartheta^2/2 - m^{(s)}D_z - M_{\text{pl}}^{(s)}, \tag{3.5}$$

where $C_1^{(s)} = \int_{z_{s-1}}^{z_s} C_{11}^{(s)}dz$, $K_1^{(s)} = \int_{z_{s-1}}^{z_s} C_{11}^{(s)}zdz$, $D_1^{(s)} = \int_{z_{s-1}}^{z_s} C_{11}^{(s)}z^2dz$, $N_{\text{pl}}^{(s)} = \int_{z_{s-1}}^{z_s} C_{11}^{(s)}\varepsilon_{xx}^{\text{pl}}dz$, $M_{\text{pl}}^{(s)} = \int_{z_{s-1}}^{z_s} C_{11}^{(s)}\varepsilon_{xx}^{\text{pl}}zdz$.

Summing (3.5) over all layers leads to constitutive equations similar to (1.9):

$$N = C_1\varepsilon + K_1\kappa + N_G + N_P + N_E, \quad M = K_1\varepsilon + D_1\kappa + M_G + M_P + M_E, \tag{3.6}$$

where

$$C_1 = \sum_s\left(C_1^{(s)} + \frac{n^{(s)}n^{(s)}}{l^{(s)}}\right), \quad K_1 = \sum_s\left(K_1^{(s)} + \frac{n^{(s)}m^{(s)}}{l^{(s)}}\right), \quad D_1 = \sum_s\left(D_1^{(s)} + \frac{m^{(s)}m^{(s)}}{l^{(s)}}\right),$$

$$N_G = \theta^2\sum_s\left(\frac{C_1^{(s)}}{2} + \frac{n^{(s)}n^{(s)}}{2l^{(s)}}\right) = \frac{C_1\theta^2}{2}, \quad M_G = \theta^2\sum_s\left(\frac{K_1^{(s)}}{2} + \frac{n^{(s)}m^{(s)}}{2l^{(s)}}\right) = \frac{K_1\theta^2}{2},$$

$$N_P = \sum_s\left(R_{\text{pl}}^{(s)}\frac{n^{(s)}}{l^{(s)}} - N_{\text{pl}}^{(s)}\right), \quad M_P = \sum_s\left(R_{\text{pl}}^{(s)}\frac{m^{(s)}}{l^{(s)}} - M_{\text{pl}}^{(s)}\right),$$

$$N_E = \sum_s\left(-\frac{n^{(s)}}{l^{(s)}}V^{(s)}\right), \quad M_E = \sum_s\left(-\frac{m^{(s)}}{l^{(s)}}V^{(s)}\right), \tag{3.7}$$

N_G, N_P, N_E and M_G, M_P, M_E are the forces and moments due to geometrical nonlinearity, physical nonlinearity, and piezoelectric properties of the material, respectively.

As Eqs. (1.9), Eqs. (3.6) and (3.7) have the most general form for materials with piezoelectric and physically nonlinear properties. For elastic piezoelectric materials and physically nonlinear passive materials, these equations are simpler, as in Sec. 1.

The inelastic strain appearing in (3.1), (3.4) and the expressions (3.5)–(3.7) for the inelastic forces and moments $N_P^{(s)}$, $M_P^{(s)}$, N_P, and M_P is determined from the uniaxial equations of the Bodner–Partom model (2.1)–(2.5) presented in [1, 2, 25].

Formulas (1.8), which, along with the bending strain, include the strain of the mid-line according to the Karman nonlinear relation, are written for the displacements u and w of the beam along the axes $\vec{Ox}$ and $\vec{Oz}$, respectively,

$$\varepsilon = \frac{\partial u}{\partial x} + \frac{1}{2}\left(\frac{\partial w}{\partial x}\right)^2.$$

Then formula (3.3) is rearranged into

$$\varepsilon_{xx} = \varepsilon + \kappa z = \frac{\partial u}{\partial x} - z\frac{\partial^2 w}{\partial x^2} + \frac{1}{2}\left(\frac{\partial w}{\partial x}\right)^2 = \frac{\partial u}{\partial x} - z\frac{\partial^2 w}{\partial x^2} + \frac{1}{2}\vartheta^2, \tag{3.8}$$

where $\vartheta = -\partial w/\partial x$ and $\kappa = \partial\vartheta/\partial x = -\partial^2 w/\partial x^2$.

The constitutive equations (3.6) and the model of a physically nonlinear material should be supplemented with the equations of motion and the following differential relations describing bending in the case of nonsmall deflections and longitudinal forces caused by these deflections:

$$\frac{\partial N}{\partial x} + q_x = \overline{\rho}\frac{\partial^2 u}{\partial t^2}, \quad \frac{\partial Q}{\partial x} + \frac{\partial N}{\partial x}\frac{\partial w}{\partial x} + N\frac{\partial^2 w}{\partial x^2} - q_z(t) = \overline{\rho}\frac{\partial^2 w}{\partial t^2}, \quad \frac{\partial M}{\partial x} - Q = 0, \tag{3.9}$$

where $\vec{q}(t) = (q_x(t), q_z(t))$ is the load uniformly distributed along the beam length and being, in the general case, a function of time; $\overline{\rho} = \sum \rho_k h_k$ is the reduced density per unit length of the beam; h_k is the thickness of the kth layer.

Note that if the longitudinal inertial effects can be neglected and the longitudinal component of the uniformly distributed load is zero, then, according to the first equation in (3.9), the longitudinal force is constant along the beam and the second equation in (3.9) becomes simpler. This fact follows from the standard large-deflection hypotheses for beams, plates, and shells and is used here to check the accuracy of the numerical scheme.

The second derivative of the displacement components with respect to time in the equations of motion for a time t_{i+1} are expressed by Newmark's formulas [25] using the displacements, velocities, and accelerations found at the previous time step.

Using Eqs. (3.6), (3.8), and (3.9), we write the governing equations describing the vibration of the beam at each time point:

$$\frac{du}{dx}=\frac{N}{C_1}-\frac{N_G+N_P+N_E}{C_1},\quad \frac{dw}{dx}=-\vartheta,\quad \frac{dM}{dx}=Q,\quad \frac{dN}{dx}=\bar{\rho}\ddot{u},$$

$$\frac{dQ}{dx}=\bar{\rho}\ddot{w}+N\left(\frac{M-M_G-M_P-M_E}{D_1}\right),\quad \frac{d\vartheta}{dx}=\frac{M-M_P+M_E}{D_1}. \tag{3.10}$$

System (3.10) yields

$$\frac{du}{dx}=\frac{N}{C_1}-\frac{N'_G}{C_1}\vartheta-\Gamma_3,\quad \frac{dw}{dx}=-\vartheta,\quad \frac{dM}{dx}=Q,\quad \frac{dN}{dx}=\bar{\rho}\left(\frac{2}{\Delta t}\right)^2 u-\Gamma_1,$$

$$\frac{dQ}{dx}=\bar{\rho}\left(\frac{2}{\Delta t}\right)^2 w+N\Gamma_5-\Gamma_2,\quad \frac{d\vartheta}{dx}=\frac{M}{D_1}-\Gamma_4, \tag{3.11}$$

where $\Gamma_1=\bar{\rho}\left[\left(\frac{2}{\Delta t}\right)^2 u^{(i)}+\frac{4}{\Delta t}\dot{u}^{(i)}+\ddot{u}^{(i)}\right]$, $\Gamma_2=\bar{\rho}\left[\left(\frac{2}{\Delta t}\right)^2 w^{(i)}+\frac{4}{\Delta t}\dot{w}^{(i)}+\ddot{w}^{(i)}\right]$, $\Gamma_3=\frac{1}{C_1}(N_P^{(i)}+N_E^{(i)})$, $\Gamma_4=\frac{M_P^{(i)}+M_E^{(i)}}{D_1}$, $\Gamma_5=\frac{M^{(i)}}{D_1}-\Gamma_4$, $N'_G=\frac{C_1}{2}\vartheta^{(i)}$, and the superscripts refer to the previous time step.

Equations (3.11) constitute the linearized system of equations (3.10) that accounts for the fact that K_1 and, hence, M_G in (3.7) are identically equal to zero for a thin-walled structural member with layers of constant thickness arranged symmetrically about the midsurface.

The system of governing equations (3.11) does not depend explicitly on time. The time is implicitly introduced by the displacements, velocities, accelerations of forces and moments of the previous time step. Moreover, N_P and M_P are integrals of the inelastic deformation history dependent, in turn, on the parameters K and β (isotropic and kinematic hardening). Therefore, the system of governing equations (3.11) and Eqs. (2.1)–(2.5) describing the behavior of the material should be solved simultaneously, adding the initial conditions

$$u=w=\vartheta=N=Q=M=0,\quad \varepsilon_{xx}^{\mathrm{pl}}=\beta=0,\quad K=K_0\quad \text{at}\quad t=0 \tag{3.12}$$

and the boundary conditions

$$u=w=0,\quad M=M(t)\quad \text{at}\quad x=0,L. \tag{3.13}$$

This problem statement is essentially nonlinear because of the nonlinearity of Eqs. (2.1)–(2.5). To solve the problem, use is made of the numerical method applied in [25] to dynamic problems of thin-walled structural members.

4. Material Properties and Problem-Solving Method. The passive material (without the piezoelectric effect) is AMg-6 aluminum alloy. Its physical and mechanical properties and Bodner–Partom parameters are the following [1, 2, 24]: ρ = 2692.65 kg/m^3, $E=0.816\cdot10^5$ МПа, $\nu=0.34$, $D_0=10^4$ sec^{-1}, $n=2.06$, $m_1=0.182$ MPa^{-1}, $m_2=3.7$ MPa^{-1}, $K_0=323.6$ MPa, $K_1=647.4$ MPa, $D_1=80$ MPa.

The physical and mechanical properties of the piezoelectric material correspond to TsTS-19 piezoceramics [8] and can be expressed using the notation of Sec. 1: $c_{11}^{\mathrm{D}} = 11.2 \cdot 10^4$ MPa, $c_{12}^{\mathrm{D}} = 6.4 \cdot 10^4$ MPa, $c_{13}^{\mathrm{D}} = 5.0 \cdot 10^4$ MPa, $c_{33}^{\mathrm{D}} = 12.5 \cdot 10^4$ MPa, $h_{31} = -5.0 \cdot 10^8$ V/m, $h_{33} = 18.0 \cdot 10^8$ V/m, $\beta_{33}^{\mathrm{S}} = 1.33 \cdot 10^8$ m/F, $\rho = 7300\,\mathrm{kg/m^3}$.

To solve the problem numerically, we use a double iterative process. The inner process is the implicit integration of the system of nonlinear evolutionary equations for inelastic strains and hardening parameters. The outer process solves the equation of motion at each time step.

The hard nonlinearity of the system of equations (2.1)–(2.5) is responsible for the ranges of fast change in the solution. Such a behavior necessitates using design models with a variable step of integration over time. The evolutionary equations are integrated using the implicit Euler method and the midpount rule. The Steffensen–Aitken procedure is used for convergence acceleration.

The linearized system of equations (3.11) is solved in the outer iterative process using the discrete-orthogonalization method and the boundary conditions (3.13) at each time step [1, 2, 25]. A practical convergence criterion is used.

The accuracy is checked by comparing the solutions of test problems to solutions obtained analytically or by other methods. For example, the solution for a homogeneous beam elastically bent by a uniformly distributed transverse load was compared with the solution obtained by the Bubnov–Galerkin method. For a hinged beam elastoplastically bent by a transverse load or moments applied to its ends, the stress and inelastic strain were plotted against the total strain. The curves were compared to experimental data and curves obtained by the FEM. The behavior of a beam with geometrical nonlinearity was compared to the results of [25]. In all these cases, the results were in good agreement.

The solution for a hinged sandwich beam having AMg-6 core layer and piezoceramic face layers of equal thickness and undergoing elastic vibration under harmonically varying moments applied to the ends and zero electric potentials applied to the electrodes was compared to the solution obtained for a nonzero electric potential. Note that the voltage causing a deflection equal to the mechanically induced one can easily be determined analytically. Indeed, if the mechanical moment $M = M_0 \sin \omega t$, then the potential difference should vary as $V^{(1)} = V_0^{(1)} \sin(\omega t + \pi) = -V_0^{(1)} \sin \omega t$, with the following equations for amplitudes being valid:

$$M_0 = M_{E0} = -\frac{H_{31}^{(1)} (h - h_1) V_0^{(1)}}{B_{33}^{(1)}}, \tag{4.1}$$

where the superscript refers to one of the piezoactive layers, and $H_{31}^{(1)}$ and $B_{33}^{(1)}$ are defined by (3.2).

These solutions are in agreement with high accuracy.

Whether the dynamic problem was solved correctly was checked against the values of the resonant frequencies for the first bending mode. The calculated results and tabulated data were in good agreement.

5. Model Problem. Consider a hinged sandwich beam with AMg-6 aluminum alloy core layer and TsTS-19 piezoceramic face layers undergoing forced vibrations. The piezoelectric layers are of equal thickness $h_1 = h_3$, the total thickness of the beam being $h = h_1 + h_2 + h_3$, where h_2 is the thickness of the aluminum layer. The beam has length $L = 0.826$ m. Two configurations are considered: (A) $h = 3$ cm, $h_1 = h_3 = 5$ mm, $h_2 = 2$ cm; (B) $h = 6$ cm, $h_1 = h_3 = 2$ mm, $h_2 = 5.6$ cm. The beam has width $b_y = 3$ cm. The resonant frequency of the first bending mode is 441 Hz for configuration A and 1167 Hz for configuration B. The excitation frequency is $f = 10$ Hz.

The piezoelectric layers are prepolarized across the thickness, and the polarization directions of the layers are opposite (for example, the upper layer is polarized in the direction of the *Oz*-axis, while the lower layer in the opposite direction).

Harmonic loading of two types is considered: moments applied to the ends of the beam and an electric potential difference applied to the electrodes of the piezolayers. In all the cases, the harmonic variation in the load was modulated by a linear function so that the set amplitude was reached in 50 vibration cycles. The deflections of the beam were symmetric about the axis since the harmonic load generated in the first quarter of a cycle induces a constant deflection component due to inelastic deformation and then vibration occurs about this bent configuration.

To analyze the mutual influence of physical and geometrical nonlinearities, it is convenient to use a stiffness characteristic for the steady-state stage of the process: dependence of the deflection amplitude on the amplitude of the bending moment. This characteristic is shown in Fig. 1 for a beam of configuration B. The dotted line corresponds to the linear case, the

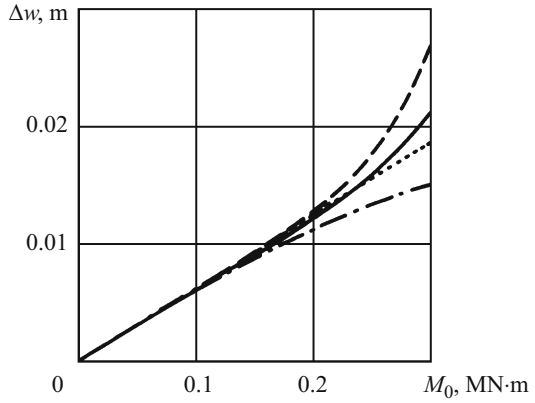

Fig. 1

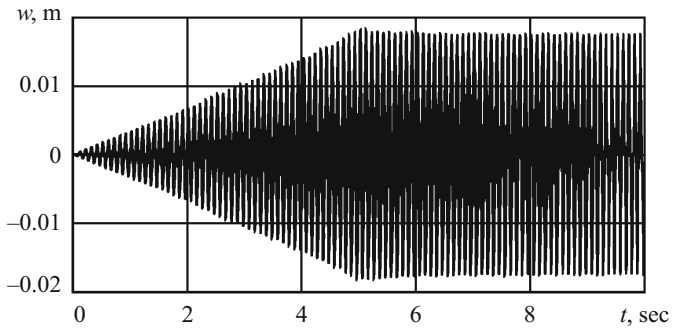

Fig. 2

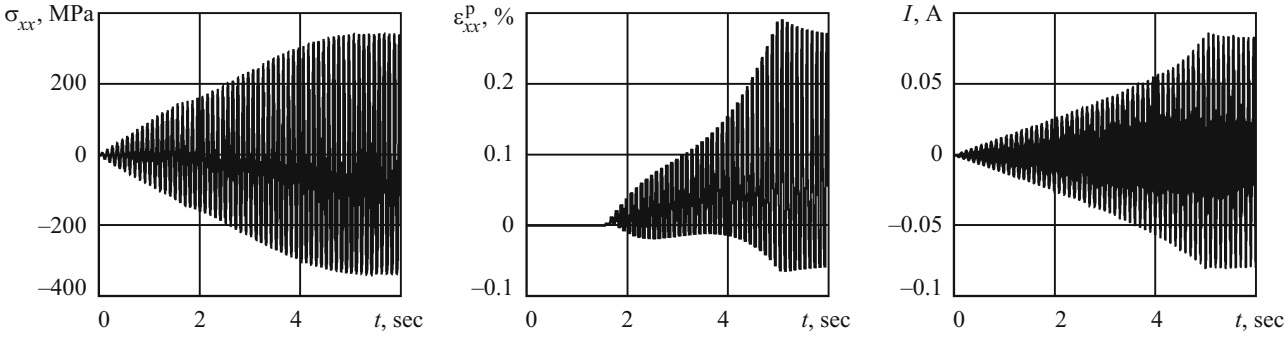

a *b* *c*

Fig. 3

dash-and-dot and dashed lines to the geometrically and physically nonlinear cases, respectively, and the solid line represents the joint effect of both nonlinearities. The physical nonlinearity is of soft type, while the geometrical nonlinearity of hard type. The effect of nonlinearities depends on the level of loading, the geometry of the beam, and the boundary conditions. It is obvious that the geometrical nonlinearity is predominant in thinner beams. The thicker the beam, the stronger the effect of the physical nonlinearity. In thick structural members, inelastic deformation may become predominant.

Figure 1 shows that there are ranges of load in which the system shows linear behavior during steady-state vibration ($M_0 < 0.12$ MN·m), the geometrical nonlinearity is predominant ($0.12 < M_0 < 0.24$ MN·m), and the effect of both nonlinearities is strong ($M_0 > 0.24$ MN·m). For a beam of configuration A, the geometrical nonlinearity is predominant in all the ranges of load.

The nonstationary response of a beam to harmonic mechanical excitation is demonstrated in Fig. 2, which shows the history of variation in the deflection of configuration B for $M_0 = 0.27$ MN·m in the presence of both physical and geometrical nonlinearities. It is seen that after first 50 cycles of vibration, when the load amplitude reaches the steady state, the deflection amplitude shows a small decrease caused by the hardening of the aluminum layers adjacent to the piezoceramics. After the completion of the transient, the cycles of vibration become symmetric about a horizontal line.

The history of variation in the stress and inelastic strain at the point $x = L/2$, $z = -h_2/2$ (the extreme lower point of the aluminum layer in the central cross-section of the beam) is presented in Figs. 3*a* and 3*b*, respectively. The evolution of the electric current in the lower piezoceramic layer as a sensor is shown in Fig. 3*c*.

The cycle of stress response is symmetric during steady-state vibration. The elastic limit of the material is reached with increasing load. This time point corresponds to the change in the envelope angle in Fig. 3*a*.

Figure 3*b* shows that in the presence of geometrical nonlinearity alone, the history of inelastic strain is not symmetric about zero because of the deformation of the beam axis. If, however, only physical nonlinearity is present, the history of inelastic deformation is symmetric. The beginning of inelastic deformation can easily be identified in Fig. 3*b*.

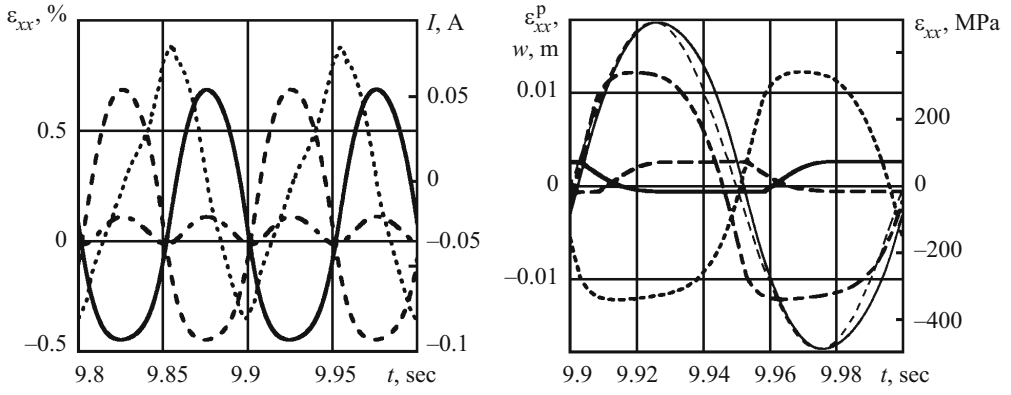

a *b*

Fig. 4

In the sensor mode, the electric current in one of the piezoelectric layers is also characterized by a cycle weakly asymmetric about zero. The reason is that the charge induced by the inverse piezoelectric effect is determined by the deformation of the piezoelectric layer, which is not symmetric about zero because of the geometrical nonlinearity.

The behavior of the electromechanical parameters within a cycle of steady-state vibration is detailed in Fig. 4.

In Fig. 4*a*, the solid and dashed lines represent the time variation in the total strains at the points ($L/2$, $-h_2/2$) and ($L/2$, $h_2/2$), respectively, and the dash-and-dot line shows the time dependence of the deformation of the beam axis, and the dotted line shows the time dependence of the current in the lower piezoelectric layer. It is seen that the asymmetry of the deformation cycles is due to the geometrical nonlinearity, particularly associated with the deformation of the beam axis. Since the axis undergoes tensile deformation, the strain of the stretched layers increases and the strain of the compressed opposite layers decreases within each half-cycle. The situation is similar for the current. It can be seen that the curves deviate from the harmonic law of variation. If the geometrical nonlinearity is disregarded, all the curves will be symmetric and the strain of the beam axis will be zero.

Figure 4*b* shows the variation in the beam deflection (thin solid line) and in the phase of the mechanical load (thin dashed line) during vibration. The heavy solid and dashed lines correspond to the inelastic strains at the points ($L/2$, $-h_2/2$) and ($L/2$, $h_2/2$) and the dotted and dash-and-dot lines to the stresses at the same points. Noteworthy is the phase shift between the mechanical load and the deflection due to the inelastic deformation of the core layer. This shift is small because so is the relative volume of the material involved in inelastic deformation.

As in Fig. 4*a*, the curves of inelastic strain and stress versus time are asymmetric about zero because of geometrical nonlinearity. With physical nonlinearity along, the curves are symmetric.

The mechanical quantities display similar behavior when vibration is electrically excited by applying a harmonically varying potential difference to the electrodes of the piezoelectric layers. Relevant curves corresponding to Figs. 2–4 have been plotted. Figure 1 is similar with the only difference that the abscissa axis indicates the amplitude of voltage V_0. Formula (4.1) can be used to establish a one-to-one correspondence between M_0 and V_0 for a special case of beam configuration. Calculations show that this formula remains valid not only in the linear range of stiffness characteristic (solid line in Fig. 1), but also in the entire range of loads considered, i.e., even in the highly nonlinear case. This fact allows easy determination of the voltage that induces a deflection equal to that caused by the mechanical moment.

This can be used, for example, for suppressing the forced mechanical vibration of an electromechanical system by applying an equivalent (in deflection) potential difference to the electrodes of the piezoelectric layers with a phase shifted by half the period of vibration.

Consider a hinged sandwich beam subjected to mechanical moments harmonically varying with time and applied to its ends. As before, the moments are linearly modulated so that the maximum is reached in 50 cycles of vibration. After the vibration becomes steady-state, a potential difference V varying as

$$V = V_0 \sin(\omega t + \pi + \delta) = -V_0 \sin(\omega t + \delta), \tag{5.1}$$

where δ is some additional phase shift, is applied at some time t_s to the electrodes of the piezoelectric layers.

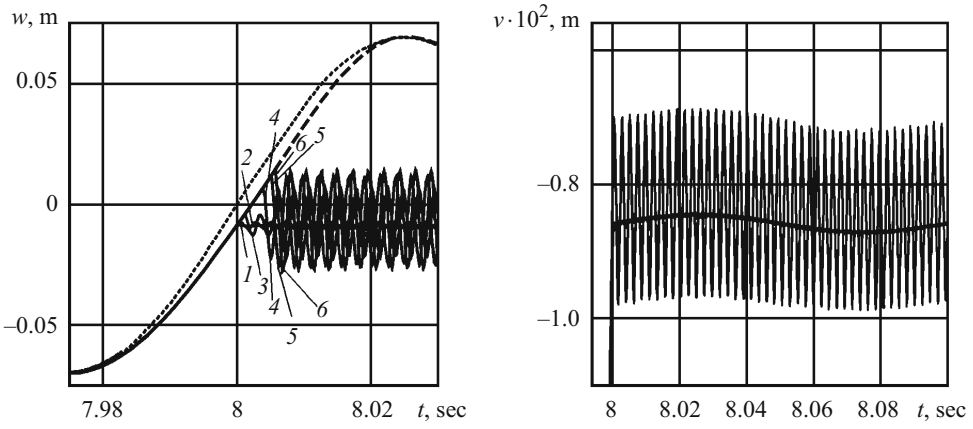

a *b*

Fig. 5

Figure 5 presents calculated results for a beam of configuration A with physical nonlinearity. In Fig. 5*a*, the dashed line represents steady-state vibration generated by moment M_0 = 100 kN·m with a frequency of 10 Hz and not suppressed by a voltage. The dashed line illustrates the phase of mechanical excitation. The solid curves represent vibration suppressed by applying voltage V_0 = 570 kV and δ = 0. Curve *1* corresponds to a quasistatic solution, and curves *2*, *3*, *4*, *5*, and *6* to dynamic solutions for t_s = 8, 8.001, 8.004, 8.005, 8.00578 sec. Figure 5*b* details the quasistatic and dynamic solutions, the heavy curve corresponding to line *1* (quasistatic solution) and the thin curve to line *6* (dynamic solution) in Fig. 5*a*. It appears that vibration cannot be completely suppressed by a voltage with a frequency of the exciting force. The residual vibration is characterized by two features.

First, it occurs about the bent position of the beam axis. This position is determined by the inelastic strains of the material and remains constant if the voltage is applied during elastic deformation (unloading or reloading in the elastic range; solid and dashed curves in Fig. 4*b*). If the inertial effects are neglected, the amplitude of residual vibration will be negligible (heavy curve in Fig. 5*b*), and vibration can completely be suppressed by a voltage with an appropriately chosen phase δ. However, the mean component remains and can be eliminated by additionally introducing a constant voltage component.

Second, dynamic effects qualitatively change the behavior of residual vibration. The vibration also occurs about the bent position of the beam axis; however, its amplitude is much higher and its frequency is equal to the natural frequency of the beam (fast components in Fig. 5) and modulated by the external load frequency equal to that of the slowly changing residual vibration. In this case, we have the equivalent problem for a bent beam having initial deflection and velocity and undergoing elastic vibration. These quantities are determined by the deviation of points of the beam from the bent position and their velocity at the time t_s the electric signal is applied. Figure 5*a* shows that the greater this deviation, the higher the amplitude of natural vibration. On the other hand, the amplitude is also dependent on the velocity of points of the beam at the time t_s.

Figure 6 demonstrates the effect of physical, and geometrical nonlinearities on the behavior of the residual vibration of a beam of configurations B for M_0 = 270 kN·m, V_0 = 670 kV. Curve *1* in Fig. 6*a* corresponds to the dynamic solution for t_s = 10.002 sec and δ = 0. Curve *2* represents the dynamic behavior of the beam for t_s = 10.002 sec and δ = δ_{Mw}, where δ_{Mw} is the phase shift between the mechanical load and the deflection caused by inelastic deformation. Curves *3* and *4* illustrate the quasistatic solution, corresponding to line *1*, in the absence and presence of geometrical nonlinearity, respectively. Curves *5a* and *6a* represent inelastic deformation at the point (L/2, $-h_2$/2) in the absence and presence of geometrical nonlinearity, and curves *5b* and *6b* show similar dependences at the point (L/2, h_2/2).

Figures 6*b* and 6*c* show the steady-state cycles of vibration after the voltage is applied. Lines *1* and *2* correspond to curves *1* and *2* in Fig. 6*a*. Line *3* represents the history of deflection for a voltage different from (5.1):

$$V = A(t)V_0 \sin(\omega t + \pi + \delta) = -A(t)V_0 \sin(\omega t + \delta),$$

$$A(t) = \begin{cases} 0, & t \le t_s, \\ (t - t_s) f / N_C, & t_s < t < t_s + N_C f, \\ 1, & t \ge t_s + N_C f, \end{cases}$$

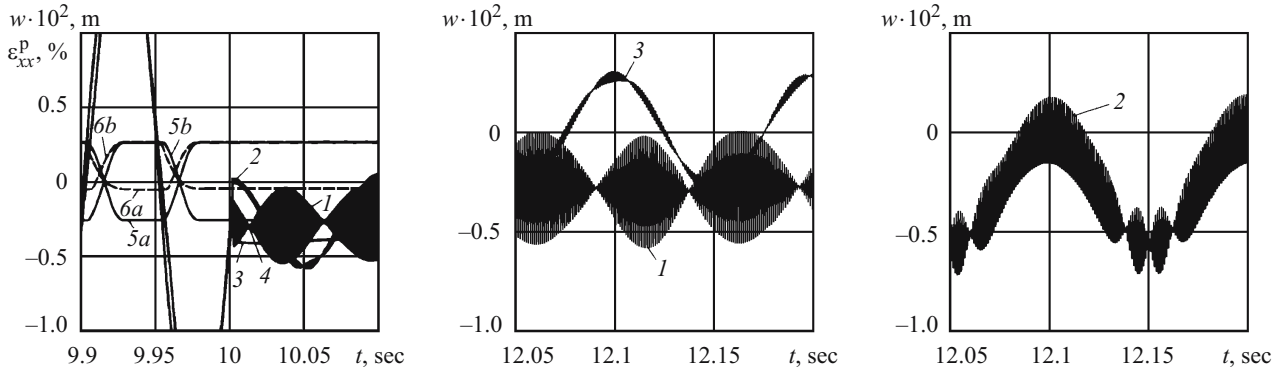

a *b* *c*

Fig. 6

where f is the frequency; N_C is the number of cycles it takes the amplitude of harmonic voltage to increases to a preset level V_0.

Curve *3* has been plotted for t_s = 10 sec and N_C = 20. The electric load with slowly increasing amplitude gradually damps the mechanical vibration, causing the amplitude of the deflection to decrease slowly. This prevents the bending of the beam axis due to inelastic deformation and the residual vibration occurs about the line $z = 0$.

Figure 6 shows that geometrical nonlinearity is manifested as two effects. First, the residual deflection of the bent beam axis decreases (lines *3* and *4* in Fig. 6*a*). This effect is due to a change in the behavior of inelastic deformation in the cross-section, which is, in turn, caused by the tension of the beam axis. Comparing curves *5* and *6* in Fig. 6*a* indicates that the beam becomes more rigid.

Second, geometrical nonlinearity is cubic in deflection. This is why the frequency spectrum of residual vibration includes odd harmonics. Since the residual vibration is elastic, there is beating in Fig. 6 resulting from the summation of vibrations at the frequency of the external load, multiple frequencies, and the frequency of the first bending resonance of the beam.

We have studied mechanical and electric vibrations of a hinged sandwich beam with piezoelectric face layers. For symmetric piezolayers with equal thickness and opposite polarization, mechanical and electric vibrations appear equivalent in both deflection and stress–strain state. This fact may be used for damping mechanical vibrations by applying an appropriate potential difference to the electrodes of the piezolayers. The physical nonlinearity of the passive layer and the geometrical nonlinearity have a strong effect on the response of the piezolayer and the entire structure. Nonlinear behavior and interaction of nonlinearities in both transient and steady-state modes hinder the complete suppression of forced vibration. Physical and geometrical nonlinearities are manifested as a phase shift between the load and the response, bending of the beam axis, and residual vibration at the natural frequency of the first bending mode and vibration with frequencies multiple to the excitation frequency. The amplitudes of residual vibration can further be decreased by using active and passive damping (additional dissipative coatings with high viscosity or electric circuits with feedback).

REFERENCES

1. Ya. A. Zhuk and I. K. Senchenkov, "Equations of a coupled dynamic thermoviscoplastic problem for thin-walled shells with piezoelectric layers," *Teor. Prikl. Mekh*., **34**, 115–121 (2001).
2. Ya. A. Zhuk and I. K. Senchenkov, "Modeling the stationary vibrations and dissipative heating of thin-walled inelastic elements with piezoactive layers," *Int. Appl. Mech*., **40**, No. 5, 546–556 (2004).
3. V. G. Karnaukhov, Ya. O. Zhuk, and T. V. Karnaukhova, "Refined thermomechanical model of a physically nonlinear shell with distributed transversely isotropic sensors undergoing forced harmonic vibration," *Dop. NAN Ukrainy*, No. 5, 70–75 (2007).

4. V. G. Karnaukhov, Ya. O. Zhuk, and T. V. Karnaukhova, "Refined thermomechanical model of a physically nonlinear shell with distributed transversely isotropic actuators undergoing forced harmonic vibration," *Dop. NAN Ukrainy*, No. 6, 50–55 (2007).
5. N. A. Shul'ga and A. M. Bolkisev, *Vibration of Piezoelectric Bodies* [in Russian], Naukova Dumka, Kyiv (1990).
6. V. T. Grinchenko, A. F. Ulitko, and N. A. Shul'ga, *Electroelasticity*, Vol. 5 of the five-volume series *Mechanics of Coupled Fields in Structural Members* [in Russian], Naukova Dumka, Kyiv (1989).
7. S. I. Pugachev (ed.), *Piezoceramic Transducers: A Handbook* [in Russian], Sudostroenie, Leningrad (1984).
8. I. K. Senchenkov and Ya. A. Zhuk, "Thermodynamic analysis of one thermoviscoplastic model," *Prikl. Mekh*., **33**, No. 2, 41–48 (1997).
9. S. Bodner and Y. Partom, "Constitutive equations for elastoviscoplastic strain hardening material," *Trans. ASME*, *J. Appl. Mech*., **42**, 385–389 (1975).
10. L. O. Grigor'eva, "Vibrations of a piezoceramic cylinder subjected to nonstationary electric excitation," *Int. Appl. Mech*., **43**, No. 3, 303–309 (2007).
11. I. A. Guz and K. P. Herrmann, "On the lower bounds for critical loads under large deformations in non-linear hyperelastic composites with imperfect interlaminar adhesion," *Eur. J. Mech.*, *A/Solids*, **22**, No. 6, 837–849 (2003).
12. V. L. Karlash, "Planar electroelastic vibrations of piezoceramic rectangular plate and half-disk," *Int. Appl. Mech*., **43**, No. 5, 547–553 (2007).
13. V. G. Karnaukhov and Ya. V. Tkachenko, "Damping the vibrations of a rectangular plate with piezoelectric actuators," *Int. Appl. Mech*., **44**, No. 2, 182–187 (2008).
14. V. G. Karnaukhov and Ya. V. Tkachenko, "Studying the harmonic vibrations of a cylindrical shell made of a nonlinear elastic piezoelectric material," *Int. Appl. Mech*., **44**, No. 4, 442–447 (2008).
15. I. F. Kirichok, "Flexural vibrations and vibrational heating of a ring plate with thin piezoceramic pads under single-frequency electromechanical loading," *Int. Appl. Mech*., **44**, No. 2, 200–207 (2008).
16. G. R. Liu, X. Q. Peng, R. Y. Lam, and J. Tani, "Vibration control simulation of laminated composite plates with integrated piezoelectrics," *J. Sound Vibr*., **220**, No. 5, 827–846 (1999).
17. S. S. Rao and M. Sunar, "Piezoelectricity and its use in disturbance sensing and control of flexible structures: A survey," *Appl. Mech. Rev*., **47**, No. 4, 113–123 (1994).
18. D. H. Robbins and J. N. Reddy, "Analysis of piezoelectrically actuated beams using a layer-wise displacement theory," *Comp. Struct*., **41**, No. 2, 265–279 (1991).
19. J. Tani, T. Takagi, and J. Qui, "Intelligent material systems: Application of functional materials," *Appl. Mech. Rev*., **51**, No. 8, 505–521 (1998).
20. H. F. Tiersten, "On the thickness expansion of the electric potential in the determination of two–dimensional equations for the vibration of electroded piezoelectric plates," *J. Appl. Phys*., **91**, No. 4, 2277–2283 (2002).
21. H. S. Tzou, *Piezoelectric Shells* (*Distributed Sensing and Control of Continua*), Kluwer, Boston–Dordrecht (1993).
22. H. S. Tzou and R. Ye, "Piezothermoelectricity and precision control of piezoelectric systems: Theory and finite element analysis," *J. Vibr. Acoust*., **116**, 489–495 (1994).
23. S. Vidoli and F. dell'Isola, "Vibration control in plates by uniformly distributed PZT actuators interconnected via electric networks," *Eur. J. Mech.*, *A/Solids*, **20**, 435–456 (2001).
24. H. Y. Zhang and Y. P. Shen, "Vibration suppression of laminated plates with 1–3 piezoelectric fiber-reinforced composite layers equipped with integrated electrodes," *Comp. Struct*., **79**, 220–278 (2007).
25. Ya. A. Zhuk and I. K. Senchenkov, "On linearization of the stiffness characteristics of flexible beams made of physically nonlinear materials," *Int. Appl. Mech*., **42**, No. 2, 196–202 (2006).